A Hierarchical Family of Three-Dimensional Potential Energy Surfaces for He-CO

Kirk A. Peterson
Washington State University, kipeters@wsu.edu

George C. McBane
Grand Valley State University, mcbaneg@gvsu.edu

A hierarchical family of three-dimensional potential energy surfaces for He-CO

Kirk A. Peterson[a)]
Department of Chemistry, Washington State University, Pullman, Washington 99164-4630

George C. McBane[b)]
Department of Chemistry, Grand Valley State University, Allendale, Michigan 49401

A hierarchical family of five three-dimensional potential energy surfaces has been developed for the benchmark He-CO system. Four surfaces were obtained at the coupled cluster singles and doubles level of theory with a perturbational estimate of triple excitations, CCSD(T), and range in quality from the doubly augmented double-zeta basis set to the complete basis set (CBS) limit. The fifth corresponds to an approximate CCSDT/CBS surface (CCSD with iterative triples/CBS, denoted CBS+corr). The CBS limit results were obtained by pointwise basis set extrapolations of the individual counterpoise-corrected interaction energies. For each surface, over 1000 interaction energies were accurately interpolated using a reproducing kernel Hilbert space approach with an $R^{-6}+R^{-7}$ asymptotic form. In each case, both three-dimensional and effective two-dimensional surfaces were developed. In standard Jacobi coordinates, the final CBS+corr surface has a global minimum at $r_{CO}=2.1322a_0, R=6.418a_0$, and $\gamma=70.84°$ with a well depth of -22.34 cm^{-1}. The other four surfaces have well depths ranging from -14.83 cm^{-1} [CCSD(T)/d-aug-cc-pVDZ] to -22.02 cm^{-1} [CCSD(T)/CBS]. For each of these surfaces the infrared spectrum has been accurately calculated and compared to experiment, as well as to previous theoretical and empirical surfaces. The final CBS+corr surface exhibits root-mean-square and maximum errors compared to experiment (^{4}He) of just 0.03 and 0.04 cm^{-1}, respectively, for all 42 transitions and is the most accurate *ab initio* surface to date for this system. Other quantities investigated include the interaction second virial coefficient, the integral cross sections, and thermal rate coefficients for rotational relaxation of CO by He, and rate coefficients for CO vibrational relaxation by He. All the observable quantities showed a smooth convergence with respect to the quality of the underlying interaction surface. © *2005 American Institute of Physics.* [DOI: 10.1063/1.1947194]

I. INTRODUCTION

The interaction of helium with carbon monoxide has been widely studied. He-CO collisions are important in the chemistry and physics of dense interstellar molecular clouds; this role motivated the important 1976 paper of Green and Thaddeus,[1] which sparked interest in the chemical physics community. The He-CO system has served as a testing ground for energy-transfer dynamics, both rotational and vibrational, and its rovibrational spectrum is a benchmark for a weakly bound van der Waals complex intermediate between the semirigid and nearly free rotor limits. Thachuk *et al.*,[2] Antonova *et al.*,[3] and Smith *et al.*[4] have reviewed experimental work on He-CO.

The first *ab initio* potential energy surface for He+CO was reported in 1980 by Thomas *et al.*[5] The Thomas, Kraemer, and Diercksen (TKD) surface was calculated using a triple-zeta basis set at the singles and doubles configuration-interaction (CISD) level of theory with the addition of the Davidson correction (CISD+Q). This surface was subsequently extended by Schinke and Diercksen[6] to include the CO stretching degree of freedom. In 1994 Chuaqui *et al.* reported the high-resolution infrared spectrum of He-CO (Ref. 7) and those results led to the development of two empirical potentials, $V_{(3,3,3)}$ and XC(fit).[7,8] While both very accurately reproduced the infrared spectrum (rms deviations of just 0.0016 and 0.0018 cm^{-1}, respectively), the XC(fit) surface was later shown[9] to yield a more accurate description of other properties of the interaction, e.g., the second virial and binary diffusion coefficients. Several subsequent studies using fourth-order Møller–Plesset perturbation theory[10–12] (MP4) indicated that the minimum-energy geometry of the complex corresponded to a skewed configuration.

One of the most accurate *ab initio* interaction surfaces to date is the symmetry-adapted perturbation theory (SAPT) surface of Heijmen *et al.*,[13] which followed the preliminary SAPT calculations of Moszynski *et al.*[14] The three-dimensional SAPT surface reproduces well the infrared spectrum of He-CO,[13] and provides an accurate description of its transport and inelastic scattering properties.[3,4,15–19]

Gianturco *et al.* reported a novel potential surface (HHSD) that was constructed by matching interaction energies obtained using density functional theory for the short-range repulsion region of the surface with long-range dispersion interactions given by the usual inverse power expansion

a)Electronic mail: kipeters@wsu.edu
b)Electronic mail: mcbaneg@gvsu.edu

with empirical dispersion coefficients.[20,21] Even more recently, a three-dimensional surface calculated at the Brueckner doubles plus perturbative triples level of theory, BD(T), with a correlation consistent triple-zeta basis set (aug-cc-pVTZ) was reported[22] and used in the calculations of the vibrational relaxation of CO by He. Lastly, Zeimen *et al.*[23] have completed a coupled cluster study, yielding a two-dimensional surface calculated at the singles and doubles coupled cluster level with perturbative triples [CCSD(T)], in conjunction with their work on the interaction of He with the $a^3\Pi$ excited state of CO. Zeimen *et al.* used a basis set that included a set of bond functions in order to efficiently describe the weak van der Waals interaction, as did the authors of two of the earlier MP4 studies.[11,12]

The initial goal of the present work was to demonstrate and test the construction of highly accurate potential energy surfaces using explicit extrapolations of calculations with sequences of correlation consistent basis sets. Previous work along these lines has been reported by one of us for the H $+H_2$,[24] O+HCl,[25,26] and O+HBr (Ref. 27) reaction systems. The He-CO van der Waals system has a well depth of slightly more than 20 cm^{-1} and detailed experimental results are available, so we expected He-CO to provide a very sensitive test of this technique. Since the CCSD(T) method is known to accurately describe weakly bound systems when paired with flexible basis sets (see, e.g., Refs. 28–30) this method was chosen for the present work. Previous CCSD(T) calculations of the electrical properties of the CO molecule have also demonstrated excellent agreement with experiment.[31] On the other hand, once the surface is accurately extrapolated to the complete basis set (CBS) limit, the remaining errors in any calculated observables, e.g., infrared transitions or vibrational relaxation rate coefficients, can be assigned to the intrinsic error of the CCSD(T) method. This has also been addressed in the present work through calculations including full iterative triples, CCSDT. The result is a hierarchical series of full three-dimensional surfaces for He-CO that smoothly range in quality, four as a function of the basis sets used at the CCSD(T) level and a final surface that also incorporates CCSDT corrections. All of the observables calculated on these surfaces, including the infrared spectrum, as well as rotational and vibrational relaxation rate coefficients, vary smoothly with potential surface quality. The details of the *ab initio* calculations, as well as the representation of the surfaces, are given in Sec. II. Section III A compares the features of the resulting surfaces with the previous ones reported in the literature. The remaining parts of this section then present the results of the calculations of the IR spectrum, interaction second virial coefficients, state-to-state integral cross sections for rotationally inelastic scattering, rotational energy transfer rate coefficients, and vibrational relaxation rate coefficients. The conclusions are summarized in Sec. IV.

II. DETAILS OF THE CALCULATIONS

Jacobi coordinates were used throughout the present work and are shown in Fig. 1. In these coordinates, r_{CO} is the CO bond length, R refers to the distance between He and the
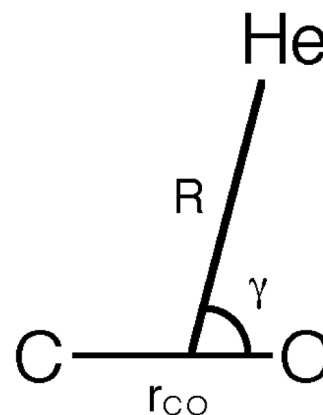

FIG. 1. Coordinate definitions.

center of mass of CO (the masses used for C and O were 12.000 and 15.994 914 63 amu, respectively), and γ is the angle between R and r_{CO} with $\gamma=180°$ referring to the HeCO configuration.

A. *Ab initio* calculations

The interaction potential energy surface of He-CO was calculated at the coupled cluster singles and doubles level of theory with a perturbative treatment of connected triple excitations, CCSD(T). In every case the interaction energies were obtained by using the full function counterpoise (CP) method.[32] The one-particle basis sets used in this work corresponded to the doubly augmented correlation consistent basis sets of Woon and Dunning,[33] d-aug-cc-pVnZ, $n=D,T,Q$. These sets are constructed from the standard aug-cc-pVnZ basis sets[34,35] by adding an additional shell of diffuse functions that are obtained as even-tempered extensions. This choice was motivated by the expectation that the very weak interaction between He and CO would be dominated by the dispersion interaction—previous calculations of the first and second hyperpolarizabilities of CO demonstrated significantly better convergence to their CBS limiting values when the d-aug basis sets were used.[31] Calculations with the d-aug-cc-pVDZ (DAVDZ) and d-aug-cc-pVTZ (DAVTZ) basis sets were carried out at all triples of the values $r_{CO} \in \{1.8,1.9,2.0,2.1322,2.2,2.4,2.6\}a_0$, $R \in \{3.0,4.0,4.5, 5.0,5.3,5.6,5.9,6.2,6.5,6.8,7.1,7.7,8.5,10,15\}a_0$, and $\gamma \in \{0,20,40,60,80,100,120,140,160,180\}°$, for a total of 1050 *ab initio* energies for each basis set.

Since the CCSD(T)/d-aug-cc-pVQZ (DAVQZ) calculations were very resource intensive, the full grid of points given above was not computed at this level. In this case only half as many points were calculated by limiting the values of γ to $0°,40°,80°,120°$, and $160°$. The full grid of energies for the DAVQZ basis set was then obtained by first forming

$$\alpha(r_{CO},R,\gamma) = \frac{E_{QZ} - E_{TZ}}{E_{TZ} - E_{DZ}} \qquad (1)$$

from the smaller grid of points, where E_{nZ} were the CCSD(T) CP-corrected interaction energies calculated with the DAVnZ basis sets. Figure 2 shows the dependence of the parameter α on R and γ for $r_{CO}=2.1322a_0$. The full grid of
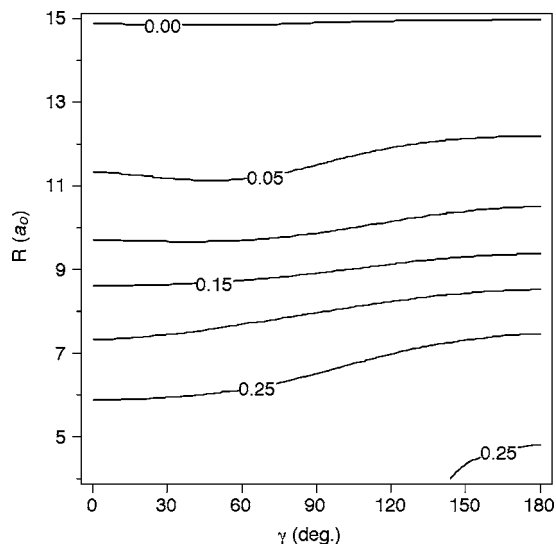
FIG. 2. Contour plot of the basis set parameter α given by Eq. (1) as a function of R and γ at a fixed $r_{CO}=2.1322a_0$.

CCSD(T)/DAVQZ energies was then obtained by first interpolating the α values over the angles γ using the reproducing kernel Hilbert space (RKHS) method[36] with an anglelike $q_2^2(x,x')$ reproducing kernel. The missing DAVQZ values were then obtained from

$$E_{QZ} = E_{TZ} + \alpha(E_{TZ} - E_{DZ}). \qquad (2)$$

The accuracy of this procedure was thoroughly tested by calculating the full grid of points in R and γ with the DAVQZ basis set for $r_{CO}=2.1322a_0$. The mean unsigned error (MUE) and root-mean-square (rms) error from using Eqs. (1) and (2) were just 0.07 and 0.14 cm^{-1}, respectively. Using a spline interpolation procedure instead of the RKHS approach resulted in average errors that were larger by factors of two to three. Lastly, in order to be consistent with the DAVQZ calculations for the other values of r_{CO}, the explicitly calculated DAVQZ energies at $\gamma=20°$, $60°,100°,140°$ and $180°$ for $r_{CO}=2.1322a_0$ were not used in constructing the full DAVQZ potential energy surface (PES); only the values obtained from Eq. (2) were used. This substitution leads to a very small change (-0.04 cm^{-1}) in the extrapolated CBS well depth and results in a smoother interpolation across the different r_{CO} values.

Even with the large d-aug-cc-pVQZ basis set, basis set incompleteness is still expected to be the major source of error in the present CCSD(T) He-CO interaction potential. In fact one of the goals of this work was to determine if pointwise basis set extrapolations over a full PES would be useful for weakly interacting systems. For this work, complete basis set limits were determined at each grid point on the surface via a three-point extrapolation[37] of the CP-corrected interaction energies:

$$E_n = E_{CBS} + Ae^{-(n-1)} + Be^{-(n-1)^2}, \qquad (3)$$

where $n=2$, 3, and 4. This function has been shown to perform very well for basis sets of these sizes (i.e., $n<5$) and is expected to yield accurate total [self-consistent field (SCF)+ correlation)] CBS limit interaction energies. A sensitive test

of this claim will be provided by the calculation of various spectroscopic and dynamical properties on the resulting CBS limit interaction PES.

After extrapolation to the CBS limit and accurate representation of the PES by an analytical form (see below), the remaining error in the PES is presumably dominated by the (small) intrinsic error in the CCSD(T) method itself. In order to account for this error in a systematic manner, CCSD(T) and CCSDT (Ref. 38) calculations were carried out with the aug-cc-pVTZ basis set for a radial cut $[R=(5-15)a_0]$ of the PES at $\gamma=63°$ and $r_{CO}=2.1322a_0$. For this fixed angle, the correlation contributions to the counterpoise-corrected interaction energies at the CCSDT level of theory differed from the CCSD(T) values by an average of 0.82% with a standard deviation of just 0.03%. For example, at $R=6.5a_0$ and $\gamma=63°$, the CCSD(T) CP-corrected binding energy with the aug-cc-pVTZ basis set is -18.34 cm^{-1}, while the CCSDT value is -18.63 cm^{-1}. At $R=6.5a_0$ and $\gamma=0°$ and $180°$, the difference in correlation contributions between CCSDT and CCSD(T) increases somewhat to 0.95% and 1.39%, respectively. We have chosen to ignore this small angle dependence in the present work, however, and the CCSD(T)/CBS interaction energies were approximately corrected to the CCSDT/ CBS level at each point by adding 0.82% of the CCSD(T)/ DAVTZ correlation contribution of the interaction energy to the CCSD(T)/CBS interaction energy. The resulting surface is denoted by CBS+corr. Of course, this procedure assumes that the basis set dependence of the difference between CCSD(T) and CCSDT is fully accounted for with the aug-cc-pVTZ basis set. In fact, CCSDT calculations with the d-aug-cc-pVDZ and aug-cc-pVTZ basis sets yielded interaction energies with nearly identical differences with respect to CCSD(T) of -0.24 and -0.29 cm^{-1}, respectively (interaction energies of -15.06 and -18.73 cm^{-1}, respectively, at the CCSDT level), so the majority of the correction is expected to be recovered with the aug-cc-pVTZ basis set. Lastly, it should be stressed that this correction is still purely *ab initio* in origin and does not involve any experimental information. All of the CCSD(T) calculations of this work used the MOLPRO suite of *ab initio* programs,[39] while the CCSDT calculations were carried out with ACES II.[40]

B. Interpolation

After making serious attempts to systematically remove all major sources of error in the calculated interaction potential, it is very important not to introduce substantial new errors when fitting or interpolating the resulting potential energy surface. In the present work, for each value of r_{CO} the interaction potential in R and γ was accurately interpolated using the RKHS method of Ho and Rabitz.[36] The R coordinate was interpolated using a [2,5] reciprocal power (RP) kernel

$$q_{RP}^{2,5}(x,x') = \frac{2}{21x_>^6}\left\{1 - \frac{3}{4}\frac{x_<}{x_>}\right\}, \qquad (4)$$

where $x_< = \min(x,x')$ and $x_> = \max(x,x')$. The kernel of Eq. (4) extrapolates in the long-range region as $-C_6/R^6 - C_7/R^7$, while at short range the kernel extrapolates as $a+bR$. The

poor extrapolation characteristics at short range, i.e., linear instead of exponential-like repulsion, compelled us to extend the *ab initio* calculations to very short distances. For instance, at the shortest value of R on the grid, $3.0a_0$, the interaction energy for $r_{CO}=2.1322a_0$ ranges from 15 000 to 113 000 cm^{-1} with the CBS+corr potential, which is well outside the area of interest for the dynamics of this system.

Ho and Rabitz[41] have pointed out that the unconstrained RKHS approach used here gives the correct qualitative behavior at long range but does not give quantitatively accurate C_6 and C_7 coefficients far beyond the range of the *ab initio* points. Since our potentials are explicitly sampled out to $15a_0$, where the interaction energy is always less than 0.5 cm^{-1}, most computed properties are unaffected by the resulting extrapolation error. To demonstrate this assertion, we tested a different RKHS scheme based on the [2,2] kernel with R^2 interpolation as suggested by Soldan and Hutson.[42] That approach yields a $-C_6/R^6-C_8/R^8$ long-range extrapolation, but affected the bound-state energy levels by less than 0.001 cm^{-1}. Nonetheless, relatively large *fractional* errors can be expected at distances beyond $20a_0$, though the *absolute* errors there are very small. Our surface is not appropriate for computation of properties that depend on the very long range behavior, such as scattering properties at temperatures well below 1 K.

The angular part of the potential was interpolated with the kernel[36]

$$q^2(y,y') = 1 + y_> y_< + 2y_<^2 y_> \left\{ 1 - \frac{1}{3} \frac{y_<}{y_>} \right\}, \qquad (5)$$

where $y=[(1-\cos\gamma)/2]$. For each value of R and γ, the r_{CO} dependence of the interaction potential was then fit to within a rms error of 0.01 cm^{-1} with a cubic polynomial in the displacement coordinate $(r_{CO}-r_e)$, where $r_e=2.1322a_0$.

The RKHS interpolation was carried out with a straightforward implementation of the algorithm described by Ho and Rabitz.[36] The fast RKHS evaluation algorithm of Hollebeek *et al.*[43] was not necessary for these modest 2D interpolations. For a single evaluation of the potential, on an R and γ grid of size $M \times N$, one first must carry out M evaluations of the distance-like kernel, and N of the angle kernel. These kernel evaluations involve conditional branches, but are otherwise simple polynomial evaluations. All the rest of the work—formation of a direct product vector of length $M \times N$, and evaluation of its dot product with a coefficient vector of the same length—are linear algebra operations that can be performed very efficiently. Our implementation forms a single direct product vector at a given R and γ, and then evaluates all seven of the required dot products in a single matrix-vector multiply whose result is the seven energies $V(r_i,R,\gamma)$.

Once those seven energies are determined, we construct the expansion coefficients $V_n(R,\gamma)$ such that

$$V(r_{CO},R,\gamma) = \sum_{n=0}^{3} V_n(R,\gamma)(r_{CO}-r_e)^n. \qquad (6)$$

They are given by $V_n(R,\gamma)=\Sigma_i G_{ni} V(r_i,R,\gamma)$, where **G** is a fitting matrix determined at the start of the program. **G** de-

TABLE I. Expectation values in atomic units of $(r_{CO}-r_e)^n$ for the low-lying vibrational states of isolated CO with $r_e=2.1322a_0$.

	$\langle (r_{CO}-r_e) \rangle_v$	$\langle (r_{CO}-r_e)^2 \rangle_v$	$\langle (r_{CO}-r_e)^3 \rangle_v$
$v=0$	0.007 76	0.004 14	0.000 12
$v=1$	0.023 32	0.012 84	0.000 77
$v=2$	0.039 07	0.022 16	0.002 11

pends only on the locations of the seven grid points in r_{CO}; it is the inverse of the design matrix **A**, where $A_{i,n}=(r_i-r_e)^n$.

C. Vibrationally averaged 2D potentials

The vibrational motion of CO is usually fast compared to other motions in the He-CO system. In that case the adiabatic decoupling approximation can be accurately invoked, whereby the r_{CO}-dependent rotational constant of CO and interaction potential function can be replaced by their vibrationally averaged quantities b_v and $\bar{V}_v(R,\gamma)$, where v labels the CO intramolecular vibrational mode.[7,13] The nuclear motion Hamiltonian for He-CO in space-fixed coordinates is then

$$H_v = -\frac{\hbar^2}{2\mu R}\frac{\partial^2}{\partial R^2} + \frac{\mathbf{l}^2}{2\mu R^2} + b_v \mathbf{j}^2 + \bar{V}_v(R,\gamma), \qquad (7)$$

where μ is the reduced mass of the complex and **j** and **l** are the angular momentum operators associated with the rotation of CO and the rotation of the He atom about the CO center of mass, respectively. The total angular momentum, $\mathbf{J=j+l}$, is always conserved, but due to the anisotropy of the potential j and l are only approximately good quantum numbers. For each of the surfaces developed in this work (DAVDZ, DAVTZ, DAVQZ, CBS, and CBS+corr), effective two-dimensional (2D), vibrationally averaged potentials $\bar{V}_v(R,\gamma)$ were constructed by replacing the terms $(r_{CO}-r_e)^n$ in Eq. (6) with their corresponding vibrational expectation values $\langle \phi_v(r_{CO})|(r_{CO}-r_e)^n|\phi_v(r_{CO})\rangle$, where $\phi_v(r_{CO})$ is a vibrational wave function of CO in vibrational state v. (Centrifugal distortion of the CO vibrational functions was not included in the 2D "effective rigid rotor" vibrationally averaged potentials; therefore no j label on the vibrational functions ϕ is required here.) The expectation values of $(r_{CO}-r_e)^n$, which are shown in Table I, were obtained using vibrational eigenfunctions calculated on a CO potential (obtained as an eight-point Lagrangian interpolation of the accurate Rydberg–Klein–Rees (RKR) potential data of Kirschner and Watson,[44] augmented by short- and long-range data from the analytical potential of Huxley and Murrell[45]) using a discrete variable representation (DVR) with a basis of sinc functions.[46]

D. Expansion of potential for dynamics calculations

For three-dimensional coupled channel calculations, radial strength functions $V_{vjv'j'\lambda}(R)$ are required such that
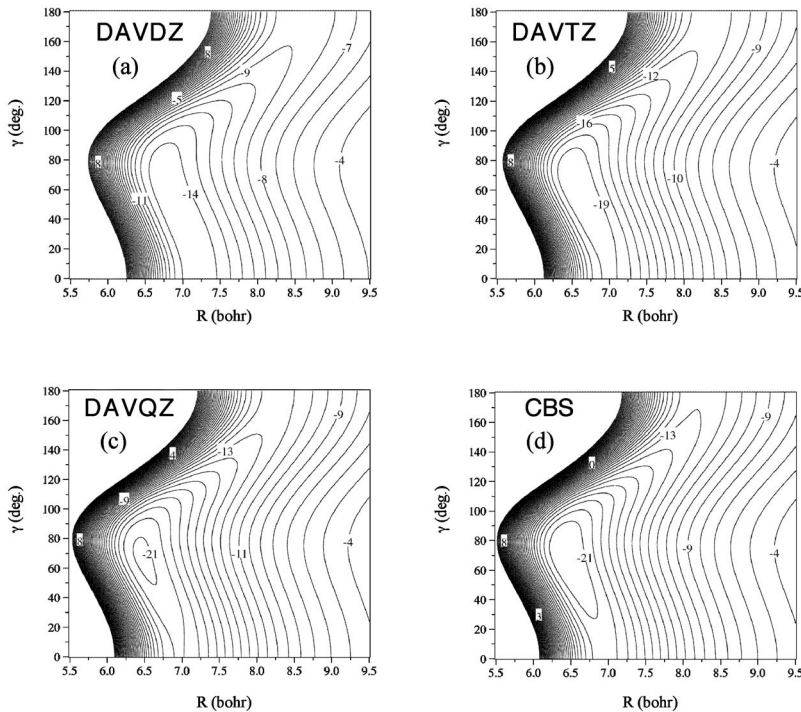
FIG. 3. Contour plots of the $R-\gamma$ dependence of the (a) DAVDZ, (b) DAVTZ, (c) DAVQZ, and (d) CBS potential energy surfaces of the present work at a fixed $r_{CO}=2.1322a_0$. The contour lines are drawn every 1 cm^{-1} with a zero of energy at separated He+CO.

$$\langle \phi_{vj}(r_{CO})|V(r_{CO},R,\gamma)|\phi_{v'j'}(r_{CO})\rangle$$

$$= \sum_{\lambda} V_{vjv'j'\lambda}(R)P_{\lambda}(\cos \gamma). \tag{8}$$

The $\phi_{vj}(r_{CO})$ are vibrational wave functions of CO in the internal state labeled by v and j, P_{λ} is a Legendre polynomial, and the angular brackets indicate integration over the diatomic bond length coordinate r_{CO}. We obtain the radial strength functions from

$$V_{vjv'j'\lambda}(R) = \sum_{n=0}^{3} R_{vjv'j'n} \sum_{k=1}^{n_{gl}} V_n(R,x_k)D_{k\lambda}, \tag{9}$$

where $x_k = \cos \gamma_k$. The **D** matrix is defined by

$$D_{k\lambda} = (\lambda + 1/2)^{1/2} P_{\lambda}(x_k)w_{k'} \tag{10}$$

where x_k and w_k are the abscissas and weights of an n_{gl}-point Gauss–Legendre quadrature in $\cos \gamma$. The **R** matrix is

$$R_{vjv'j'n} = \langle \phi_{vj}(r)|(r-r_e)^n|\phi_{v'j'}(r)\rangle. \tag{11}$$

The elements of **R** were calculated in advance using the LEVEL program of Le Roy,[47] using a potential curve computed from the CO molecular constants of Maki et al.[48] with Le Roy's RKR program.[49] (It is a historical artifact that different CO potentials were used here and in Sec. II C. We have checked that the two potentials are sufficiently similar that none of our reported dynamical results depend on which is used.)

III. RESULTS

A. Features of the potential energy surfaces

As shown in Fig. 3 for a fixed CO bond length, the potential energy surfaces of the present work have a single global minimum located in a skewed configuration interme-

diate between linear CO–He and a T-shaped geometry. The equilibrium geometries and well depths for each of these surfaces are also shown in Table II, where they are compared to the properties of the other surfaces in the literature. Both the equilibrium geometry and well depth smoothly change as a function of basis set; the He-CO center of mass separation decreases (R shrinks from $7.02a_0$ to $6.43a_0$), the geometry becomes more skewed (the Jacobi angle γ increases from about 36° to 71°), and the well depth decreases from -14.83 cm^{-1} at the DAVDZ level to -22.02 cm^{-1} at the CBS limit. As expected, the largest change occurs between DAVDZ and DAVTZ, and comparison of Figs. 3(a)–3(d) indicates that the repulsive wall is already well represented at the DAVTZ level. Basis set extrapolation results in nonnegligible changes between the DAVQZ and CBS surfaces; in particular, the well becomes deeper by nearly 0.8 cm^{-1}. Finally, the addition of the correction for iterative triple excitations has only a minor effect on the properties of the minimum, i.e., the He-CO separation shortens by just $0.008a_0$ and the well depth decreases by 0.32 cm^{-1}.

The CBS and CBS+corr surfaces have shorter equilibrium R and larger equilibrium γ values than any of the other surfaces in the literature. The barrier to linearity is very small in the complex, as mentioned in several of the earlier studies, so small differences among the studies produce equilibrium skew angles varying from 0° to nearly 71°. Our best estimate of the well depth is that on the CBS+corr surface, -22.34 cm^{-1}; it compares very well to those of the V_{333} and XC(fit) potentials[7,8] (-22.91 and -22.53 cm^{-1}, respectively), which were fit to the high-resolution infrared data. The well of the SAPT potential[13] appears to be a cm^{-1} or more too deep, while both the BD(T) surface of Kobayashi et al.[22] and the recent CCSD(T) surface of Zeimen et al.[23] are too shallow due mainly to basis set truncation errors. Given the method of its construction, the HHSD surface[20] yields sur-

TABLE II. Geometries (a_0 and degrees) and well depths (cm^{-1}) of the global minimum on the final He-CO interaction surfaces of this work compared to those of previous surfaces (for $r_{CO}=2.132a_0$).

PES	R	γ	ΔE
DAVDZ	7.015	36.10	−14.83
DAVTZ	6.551	62.95	−19.94
DAVQZ	6.466	68.18	−21.27
CBS	6.426	70.81	−22.02
CBS+corr	6.418	70.84	−22.34
TKD[a]	7.0/6.8	30/90	−17/−16
MP4[b]	6.43	70	−21.9
MP4[c]	6.60	60	−20.32
V_{333}[d]	6.41	121	−22.91
XC(fit)[e]	6.84	0	−22.53
SAPT[f]	6.53	48.4	−23.73
HHSD[g]	6.71	32.8	−21.81
BD(T)[h]	6.77	40.8	−18.60
CCSD(T)[i]	6.48	69	−21.35

[a]Reference 5. Both minima are shown.
[b]Reference 11.
[c]Reference 12.
[d]Reference 7.
[e]Reference 8. This potential has a nearly equivalent minimum at $\gamma=90°$, and the energy varies by less than 1 cm^{-1} between 0° and 90°.
[f]Reference 13.
[g]References 21 and 83.
[h]Reference 22.
[i]Reference 23.

prisingly accurate equilibrium properties. The infrared spectrum calculated from this surface,[21] however, exhibited errors nearly an order of magnitude larger than those arising from either SAPT (Ref. 13) or some of the more accurate surfaces of the present work (see below). This observation reinforces the difficulty of assessing the accuracy of a given potential surface based on only one type of property.[9]

In order to better understand the role of electron correlation and basis set on the well depth of the He-CO complex, a series of calculations at a fixed geometry were undertaken at both the CCSD and CCSD(T) levels of theory with basis sets ranging from aug-cc-pVDZ to aug-cc-pV5Z and d-aug-cc-pVDZ to d-aug-cc-pV5Z. The resulting total energies, counterpoise-corrected well depths, and basis set superposition errors (BSSEs) are shown as a function of basis set in Table III. For both the CCSD and CCSD(T) methods the binding energy increases and the BSSE decreases as the basis set is increased towards the CBS limit. Use of the doubly augmented basis sets tends to roughly double the BSSE, but increases the well depth by more than 1 cm^{-1}. The effect of triple excitations, i.e., CCSD(T) - CCSD, amounts to about 4.4 cm^{-1} with the d-aug-cc-pV5Z basis set, which is very

TABLE III. Dependence of the well depth on basis set for CCSD and CCSD(T).

Method	Basis set	Geometry[a]	$E(cm^{-1})$	$\Delta E(cm^{-1})$[b]	BSSE (cm^{-1})[c]
CCSD	aug-cc-pVDZ	DAVDZ	−115.950 655 5	−11.22	−17.10
	aug-cc-pVTZ	DAVTZ	−116.045 209 6	−14.76	−5.42
	aug-cc-pVQZ	DAVQZ	−116.074 227 9	−15.85	−2.66
	aug-cc-pV5Z	DAVQZ	−116.083 341 4	−16.54	−1.15
	d-aug-cc-pVDZ	DAVDZ	−115.952 028 5	−12.50	−32.01
	d-aug-cc-pVTZ	DAVTZ	−116.046 156 8	−16.05	−16.16
	d-aug-cc-pVQZ	DAVQZ	−116.074 631 0	−16.88	−5.33
	d-aug-cc-pV5Z	DAVQZ	−116.083 507 2	−17.25	−2.66
CCSD(T)	aug-cc-pVDZ	DAVDZ	−115.962 972 5	−13.34	−18.08
	aug-cc-pVTZ	DAVTZ	−116.062 774 6	−18.44	−5.66
	aug-cc-pVQZ	DAVQZ	−116.092 982 0	−20.02	−2.80
	aug-cc-pV5Z	DAVQZ	−116.102 563 4	−20.84	−1.23
	CBS (2-4)[d]			−20.91	
	CBS(3-5)[e]			−21.13	
	d-aug-cc-pVDZ	DAVDZ	−115.964 511 2	−14.82	−34.02
	d-aug-cc-pVTZ	DAVTZ	−116.063 778 9	−19.93	−16.69
	d-aug-cc-pVQZ	DAVQZ	−116.093 412 8	−21.21	−5.56
	d-aug-cc-pV5Z	DAVQZ	−116.102 742 2	−21.66	−2.80
	CBS (2-4)[d]			−21.90	
	CBS(3-5)[e]			−21.91	
	CBS(4,5)[f]			−22.12	

[a]Geometries used were taken from the CCSD(T) PES parameters given in Table II.
[b]Counterpoise-corrected interaction energy.
[c]Basis-set superposition error removed by the counterpoise correction.
[d]Based on an extrapolation of DZ, TZ, and QZ basis sets using Eq. (3).
[e]Based on an extrapolation of TZ, QZ, and 5Z basis sets using Eq. (3).
[f]Based on an extrapolation of QZ and 5Z basis sets using a n^{-3} extrapolation. See the text.

close to the CBS limit. As shown previously in Table II, the difference between CCSD(T) and CCSDT amounts to less than 10% of this contribution and the impact of connected quadruple excitations, i.e., from CCSDTQ calculations, is expected to be even less than this. Table III also shows the results of several basis set extrapolations using different combinations of correlation consistent basis sets. Obviously the singly augmented basis sets do not become sufficiently diffuse to yield very accurate CBS limits for the well depth, i.e., both the CBS(2-4) and CBS(3-5) values appear to be too shallow by about 1 cm^{-1}. In the case of the d-aug basis sets, use of the DAVDZ through DAVQZ sets or DAVTZ through DAV5Z basis sets yields essentially identical CBS extrapolated well depths when Eq. (3) is used. Also shown in Table III is the result of using the simple two-point $1/n^3$ formula of Helgaker *et al.*[50] on the total interaction energies. The well depth obtained with this alternative formula is only 0.2 cm^{-1} lower than that of Eq. (3). Thus, these calculations tend to confirm that the well depth of our final CBS+corr surface, -22.34 cm^{-1}, is probably accurate to within 0.2 cm^{-1} and perhaps lies slightly above (smaller in magnitude than) the true well depth of this system.

B. Infrared spectrum

Using the 2D vibrationally averaged potentials, the energies of the bound states of He-CO for $v=0$ and 1 were accurately determined using a coupled channel approach with the BOUND program of Hutson.[51] The rotational basis set included CO rotational levels up to $j=18$, and the diabatic modified log-derivative method of Manolopoulos was used with step sizes of 0.03 and 0.06 Å that were extrapolated to zero step size to yield the final eigenvalues. In all cases the propagation was carried out from $R=1.5$ to 40.0 Å in order to ensure convergence of the highest-lying bound levels. Reduced masses of 3.501 913 38 (^{4}He-CO) and 2.722 699 550 (^{3}He-CO) amu were used with CO rotational and centrifugal distortion constants of $B_0=1.922\,528\,960\,4$ cm^{-1}, B_1

$=1.905\,025\,96$ cm^{-1}, $D_0=6.121\,085\,27\times10^{-6}$ cm^{-1}, and D_1 $=6.120\,543\times10^{-6}$ cm^{-1}. The latter values were derived from the accurate Dunham expansions of Le Floch[52] and Maki *et al.*[48]

Within the adiabatic decoupling approximation, the individual infrared transitions are given by

$$v(v=1,j',l',J' \leftarrow v=0,j'',l'',J'') = E^{J'}_{j',l',v=1} - E^{J''}_{j'',l'',v=0}$$
$$+ Q_1(0), \qquad (12)$$

where $Q_1(0)=2143.2457$ cm^{-1} is the frequency of the CO fundamental band origin.[53] The selection rules for the intermolecular transitions accompanying the fundamental transition of CO are $|\Delta p|=1$ with $(-1)^p=(-1)^{j+l}$ and $|\Delta J|=0$ or 1. Energy levels greater than zero with parity $p=(-1)^{J+1}$ are truly bound if they lie below the $j=1$ rotational state of CO (3.8450 cm^{-1} in $v=0$) since these states cannot mix with $j=0$ continuum states, which have parity $p=(-1)^J$.

Energy levels calculated on each of the surfaces of this work are shown in Tables IV–VI for ^{4}He-CO($v=0$), ^{4}He-CO($v=1$), and ^{3}He-CO, respectively, where they are also compared to the accurate values (uncertainties of about 0.001 cm^{-1}) derived from experiment.[7,53–55] Table VII summarizes the errors compared to experiment for the infrared transitions of ^{4}He-CO accompanying the fundamental vibrational band of CO. Since the well is much too shallow on the DAVDZ surface, only about half of the total number of energy levels are supported and the error is as large as 0.34 cm^{-1} among the possible transitions. Nearly all the experimental bound levels are present on the DAVTZ surface, but the errors are dominated by transitions among the higher-lying levels, resulting in average and maximum errors similar to the DAVDZ case. The accuracy is much improved, however, at the DAVQZ level and particularly after extrapolation to the CBS limit. For the latter surface both the rms error (0.04 cm^{-1}) and maximum unsigned error (0.09 cm^{-1}) are nearly identical to those obtained using the SAPT surface of Ref. 13. As shown in Fig. 4, while the energy-level dif-
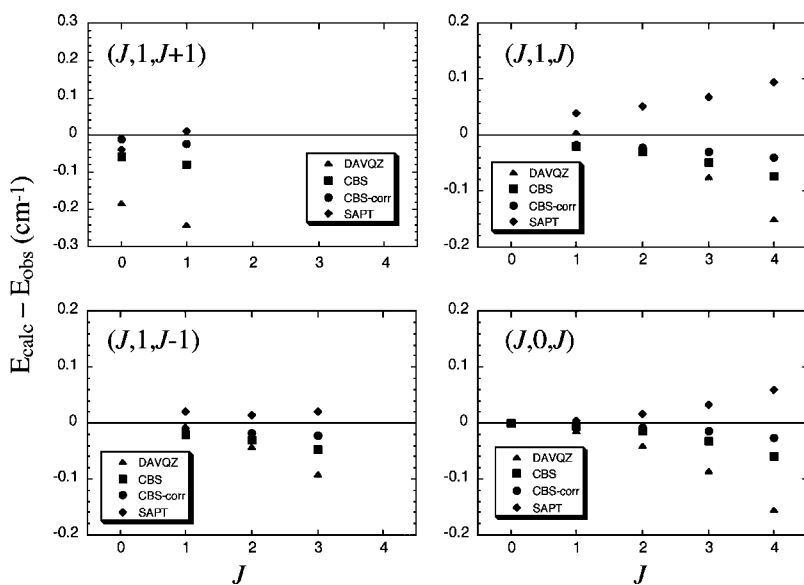

FIG. 4. Errors (in cm^{-1}) in the calculated energy levels of the ^{4}He-CO complex as a function of the total angular momentum J in $v=0$ for three interaction potentials of the present work compared to results using the SAPT potential of Ref. 13. The levels are grouped by (J,j,l).

TABLE IV. Energy levels (in cm^{-1}) of the ^{4}He-CO complex for $v=0$, relative to the $(J,j,l)=(0,0,0)$ level at −3.2493 (DAVDZ), −5.3242 (DAVTZ), −5.9286 (DAVQZ), −6.2730 (CBS), and −6.4308 cm^{-1} (CBS+corr).

J	(j,l)	DAVDZ	DAVTZ	DAVQZ	CBS	CBS+corr	Expt.[a]
0	(0,0)	0	0	0	0	0	0
	(1,1)	...[b]	4.9649	5.2089	5.3322	5.3781	5.3909
1	(0,1)	0.4836	0.5474	0.5630	0.5715	0.5741	0.5763
	(1,0)	...[b]	3.9970	3.9893	3.9753	3.9796	3.9954
	(1,1)	4.2534	4.2982	4.2714	4.2481	4.2496	4.2677
	(1,2)	...[b]	...[b]	5.8538	6.0157	6.0724	6.0955
2	(0,2)	1.4291	1.6282	1.6759	1.7019	1.7101	1.7171
	(1,1)	...[b]	4.6526	4.6922	4.7040	4.7165	4.7342
	(1,2)	5.2226	5.4102	5.4197	5.4162	5.4239	5.4466
3	(0,3)	2.7785	3.2093	3.3090	3.3628	3.3803	3.3945
	(1,2)	...[b]	...[b]	5.8426	5.8879	5.9112	5.9336
	(1,3)	6.6038	7.0323	7.1002	7.1285	7.1463	7.1760
4	(0,4)	...[b]	5.2177	5.4006	5.4974	5.5300	5.5556
	(1,4)	...[b]	...[b]	9.2427	9.3197	9.3537	9.3934

[a]References 7 and 53–55.
[b]This level was not supported by this potential.

TABLE V. Energy levels (in cm^{-1}) of the ^{4}He-CO complex for $v=1$, relative to the $(J,j,l)=(0,0,0)$ level at −3.2617 (DAVDZ), −5.3456 (DAVTZ), −5.9517 (DAVQZ), −6.2971 (CBS), and −6.4552 cm^{-1} (CBS+corr).

J	(j,l)	DAVDZ	DAVTZ	DAVQZ	CBS	CBS+corr	Expt.[a]
0	(0,0)	0	0	0	0	0	0
	(1,1)	...[b]	4.9448	5.1819	5.3025	5.3475	5.3594
1	(0,1)	0.4831	0.5468	0.5623	0.5708	0.5735	0.5764
	(1,0)	...[b]	3.9650	3.9567	3.9424	3.9467	3.9640
	(1,1)	4.2199	4.2663	4.2391	4.2156	4.2172	4.2365
	(1,2)	...[b]	...[b]	5.8410	5.9942	6.0483	6.0700
2	(0,2)	1.4279	1.6265	1.6741	1.7001	1.7083	1.7161
	(1,1)	...[b]	4.6202	4.6590	4.6703	4.6828	4.7015
	(1,2)	5.1885	5.3775	5.3867	5.3829	5.3906	5.4147
3	(0,3)	2.7770	3.2064	3.3058	3.3596	3.3770	3.3917
	(1,2)	...[b]	...[b]	5.8095	5.8540	5.8772	5.9000
	(1,3)	6.5694	6.9987	7.0664	7.0943	7.1121	7.1432
4	(0,4)	...[b]	5.2146	5.3967	5.4932	5.5257	5.5509
	(1,4)	...[b]	...[b]	9.2085	9.2852	9.3191	9.3604

[a]References 7 and 53–55.
[b]This level was not supported by this potential.

TABLE VI. Energy levels (in cm^{-1}) of the ^{3}He-CO complex, relative to the $(J,j,l)=(0,0,0)$ level at −5.0833 (CBS) and −5.2236 cm^{-1} (CBS+corr) for $v=0$, and −5.1058 (CBS) and −5.2465 cm^{-1} (CBS+corr) for $v=1$.

J	(j,l)	$v=0$			$v=1$		
		CBS	CBS+corr	Expt.	CBS	CBS+corr	Expt.[a]
0	(0,0)	0	0	0	0	0	0
	(1,1)	5.0552	5.1425	5.1775	5.0558	5.1332	5.1629
1	(0,1)	0.6928	0.6966	0.7003	0.6922	0.6959	0.6997
	(1,0)	3.9571	3.9625	3.9748	3.9242	3.9296	3.9423
	(1,1)	4.3659	4.3679	4.3843	4.3330	4.3351	4.3518
2	(0,2)	2.0530	2.0648	2.0738	2.0514	2.0631	2.0721
	(1,1)	4.7690	4.7843	4.8004	4.7362	4.7513	4.7673
	(1,2)	5.7745	5.7853	5.8069	5.7411	5.7520	5.7735
3	(0,3)	4.0151	4.0417	4.0608	4.0130	4.0393	4.0582
	(1,3)	7.7995	7.8261	7.8560	7.7660	7.7925	7.8233

[a]References 7, 53, and 54.

TABLE VII. Errors (in cm^{-1}) in the calculated infrared transition frequencies of ^{4}He-CO accompanying the fundamental vibrational band of CO. For comparison, the V_{333} (Ref. 7) and XC(fit) (Ref. 8) potentials, which were fitted to the infrared data, had rms errors of 0.016 and 0.018 cm^{-1}, respectively.

	DAVDZ (14)[b]	DAVTZ (22)[b]	DAVQZ (28)[b]	CBS (28)[b]	CBS+corr (28)[b]	SAPT[a] (28)[b]
rms error	0.15	0.17	0.09	0.04	0.03	0.04
Max. unsigned error	0.34	0.44	0.22	0.09	0.04	0.10

[a]Reference 13.
[b]Values denote the number of levels supported by this potential for $v=0$.

ferences between theory and experiment for the CBS and SAPT surfaces are very similar, the distributions of the errors are not. In general, the energy levels calculated on the DAVQZ and CBS surfaces lie below experiment while those on the SAPT surface are too high. Lastly, the CBS+corr surface yields nearly the same rms error as the CBS surface, but the maximum error is cut in half to just 0.04 cm^{-1}, which is essentially the same as the rms error (0.03 cm^{-1}). Figure 4 demonstrates that the improvement is mainly in the energy levels near dissociation. All the calculated infrared transitions from the CBS+corr potential surface are compared to experiment in Table VIII for ^{4}He-CO and Table IX for ^{3}He-CO.

To verify the accuracy of bound state calculations on the effective 2D potentials, we also performed two limited sets of fully converged three-dimensional (3D) calculations. The first set tested the $J=0$ results for both $v=0$ and $v=1$ using the CBS potential surface. These calculations used the variational truncation-recoupling scheme described in Ref. 56. A total of 7000 3D basis functions were used to converge the lowest two states in both vibrational levels. The 3D basis was constructed by recoupling five one-dimensional (1D) wave functions for r_{CO} defined on an interval from $1.4a_0$ to $5.0a_0$ with 1400 2D wave functions in (R,γ) coordinates, where R ranged from $3a_0$ to $40a_0$. The 2D wave functions were obtained by diagonalization of a reference 2D Hamiltonian in a direct product basis of 70 R by 20 γ wave functions. Atomic masses of 4.002 603 24 amu for ^{4}He, 15.994 914 63 amu for ^{16}O, and 12.00 amu for ^{12}C were used. The results agreed with the $J=0$ energies listed in Tables IV and V to within 10^{-3} cm^{-1}.

A second set of 3D calculations was carried out in BOUND for ^{4}He-CO with both the CBS and CBS+corr potential surfaces for all J in $v=0$. These calculations used the radial strength functions defined by Eq. (9). None of the results differed from the energies listed in Table IV by more than 10^{-4} cm^{-1}.

C. Interaction second virial coefficients

Second virial coefficients for the He-CO interaction have been measured by Brewer[57] and by Schramm *et al.*[58] In the range of temperatures where the measurements overlap, the two data sets are in excellent agreement. Schramm *et al.* measured two additional values at lower temperatures.

The second virial coefficients are sensitive to the depth and volume of the attractive well at low temperatures, and to

the volume of the repulsive core at high temperatures. They are spherically averaged quantities and are not very sensitive to anisotropy.

TABLE VIII. Transition frequencies (in cm^{-1}) in the infrared spectrum of ^{4}He-CO accompanying the fundamental band of CO.

$(J',j',l')\leftarrow(J'',j'',l'')$	CBS+corr	Expt.[a]	$\nu_{\text{theory}}-\nu_{\text{expt.}}$
$(1,1,1)\leftarrow(1,1,0)$	2143.4589	2143.4861	−0.027
$(1,1,0)\leftarrow(1,1,1)$	2142.9184	2142.942	−0.024
$(1,1,1)\leftarrow(1,1,2)$	2141.3660	2141.3865	−0.021
$(2,1,2)\leftarrow(2,1,1)$	2143.8954	2143.9265	−0.031
$(2,1,1)\leftarrow(2,1,2)$	2142.4802	2142.5002	−0.020
$(3,1,3)\leftarrow(3,1,2)$	2144.4222	2144.4557	−0.033
$(3,1,2)\leftarrow(3,1,3)$	2141.9521	2141.9698	−0.018
$(1,0,1)\leftarrow(0,0,0)$	2143.7948	2143.8227	−0.028
$(1,1,0)\leftarrow(0,1,1)$	2141.7899	2141.8185	−0.029
$(1,0,1)\leftarrow(0,1,1)$	2138.4166	2138.4315	−0.015
$(2,1,1)\leftarrow(1,0,1)$	2147.3299	2147.3709	−0.041
$(2,0,2)\leftarrow(1,0,1)$	2144.3555	2144.3852	−0.030
$(2,1,1)\leftarrow(1,1,2)$	2141.8316	2141.8516	−0.020
$(2,0,2)\leftarrow(1,1,0)$	2140.950	2140.9656	−0.016
$(2,0,2)\leftarrow(1,1,2)$	2138.8572	2138.8665	−0.009
$(3,1,2)\leftarrow(2,0,2)$	2147.3883	2147.4290	−0.041
$(3,0,3)\leftarrow(2,0,2)$	2144.8882	2144.9202	−0.032
$(3,0,3)\leftarrow(2,1,1)$	2141.8818	2141.9031	−0.021
$(4,0,4)\leftarrow(3,0,3)$	2145.3666	2145.4024	−0.036
$(4,0,4)\leftarrow(3,1,2)$	2142.8357	2142.8628	−0.027
$(0,1,1)\leftarrow(1,0,1)$	2147.9946	2148.0289	−0.034
$(0,1,1)\leftarrow(1,1,0)$	2144.5892	2144.6096	−0.020
$(0,0,0)\leftarrow(1,0,1)$	2142.6471	2142.6698	−0.023
$(1,1,2)\leftarrow(2,0,2)$	2147.5594	2147.5983	−0.039
$(1,1,0)\leftarrow(2,0,2)$	2145.4578	2145.4924	−0.035
$(1,1,2)\leftarrow(2,1,1)$	2144.5531	2144.5818	−0.029
$(1,0,1)\leftarrow(2,0,2)$	2142.0846	2142.1049	−0.020
$(1,0,1)\leftarrow(2,1,1)$	2139.0782	2139.0877	−0.009
$(2,1,1)\leftarrow(3,0,3)$	2144.5237	2144.5531	−0.029
$(2,0,2)\leftarrow(3,1,2)$	2139.0184	2139.0281	−0.010
$(3,1,2)\leftarrow(4,0,4)$	2143.5684	2143.5898	−0.021
$(3,0,3)\leftarrow(4,0,4)$	2141.0683	2141.0822	−0.014
$(0,0,0)\leftarrow(1,1,0)$	2139.2417	2139.2502	−0.009
$(4,0,4)\leftarrow(4,1,4)$	2139.3932	2139.4032	−0.010
$(3,0,3)\leftarrow(3,1,3)$	2139.452	2139.4613	−0.009
$(2,0,2)\leftarrow(2,1,2)$	2139.5057	2139.5154	−0.010
$(1,0,1)\leftarrow(1,1,1)$	2139.5452	2139.5543	−0.009
$(1,1,1)\leftarrow(1,0,1)$	2146.8643	2146.9061	−0.042
$(2,1,2)\leftarrow(2,0,2)$	2146.9018	2146.9433	−0.042
$(3,1,3)\leftarrow(3,0,3)$	2146.9530	2146.9943	−0.041
$(4,1,4)\leftarrow(4,0,4)$	2147.0103	2147.0506	−0.040
$(1,1,0)\leftarrow(0,0,0)$	2147.1680	2147.2098	−0.042

[a]References 7, 54, and 55.

TABLE IX. Transition frequencies (in cm^{-1}) in the infrared spectrum of ^{3}He-CO accompanying the fundamental band of CO.

$(J',j',l') \leftarrow (J'',j'',l'')$	CBS+corr	Expt.[a]	$\nu_{theory} - \nu_{expt}$
$(1,0,1) \leftarrow (0,0,0)$	2143.921	2143.9489	−0.028
$(1,0,1) \leftarrow (0,1,1)$	2138.7785	2138.7701	0.008
$(2,1,1) \leftarrow (1,0,1)$	2147.2798	2147.3152	−0.035
$(2,0,2) \leftarrow (1,0,1)$	2144.5916	2144.6192	−0.028
$(3,0,3) \leftarrow (2,0,2)$	2145.1996	2145.2323	−0.033
$(0,1,1) \leftarrow (1,0,1)$	2147.6617	2147.7105	−0.049
$(0,0,0) \leftarrow (1,0,1)$	2142.5285	2142.5489	−0.020
$(1,0,1) \leftarrow (2,0,2)$	2141.8562	2141.8728	−0.017
$(1,0,1) \leftarrow (2,1,1)$	2139.1367	2139.1471	−0.010
$(2,0,2) \leftarrow (3,0,3)$	2141.2464	2141.2593	−0.013
$(2,1,2) \leftarrow (2,1,1)$	2144.1927	2144.2203	−0.028
$(2,1,1) \leftarrow (2,1,2)$	2142.1910	2142.2080	−0.017
$(0,0,0) \leftarrow (1,1,0)$	2139.2626	2139.2728	−0.010
$(3,0,3) \leftarrow (3,1,3)$	2139.4382	Not obs.	-
$(2,0,2) \leftarrow (2,1,2)$	2139.5028	2139.5133	−0.010
$(1,0,1) \leftarrow (1,1,1)$	2139.5531	2139.5633	−0.010
$(1,1,1) \leftarrow (1,0,1)$	2146.8635	2146.8994	−0.036
$(2,1,2) \leftarrow (2,0,2)$	2146.9122	2146.9478	−0.036
$(3,1,3) \leftarrow (3,0,3)$	2146.9759	2147.0105	−0.035
$(1,1,0) \leftarrow (0,0,0)$	2147.1546	2147.1903	−0.036

[a]References 7 and 54.

We computed the virial coefficients with a Wigner–Kirkwood expansion using the prescriptions of Pack[59] and of Hirschfelder *et al.*[60] We included the first-order radial and angular quantum corrections, and the second-order radial correction. The second-order radial correction was always negative and was less than 0.15 cm^3/mol in magnitude at all $T \geqslant 70$ K.

Figure 5 shows the virial coefficients computed from several potentials and the experimental results. The upper panel shows the convergence of the computed coefficients with basis set size. Over the whole temperature range of the measurements the results converge smoothly. The DZ results are most in error at low temperature; that is to be expected since the DZ calculations give a relatively poor description of the attractive well.

The lower panel shows the effect of the full-triples correction and compares the best present potentials with results from the XC(fit) and SAPT potentials. The full-triples correction has a relatively small effect. The CBS+corr results are almost identical to those from the XC(fit) potential. The SAPT potential gives results that are lower by 1–2 cm^3/mol over the temperature range. That difference reflects the slightly deeper SAPT well. The experimental uncertainties are large enough that the data cannot discriminate among the different potentials.

All the potentials, including the XC(fit) and SAPT potentials, give virial coefficients larger than the two measured coefficients at temperatures below 100 K. The disagreement could come from errors that are common to all the potentials or from experimental errors larger than those stated. The classical part B_{cl} is a lower bound on the quantum result for a given potential;[61,62] the upper panel of Fig. 5 shows the classical results from the CBS+corr and SAPT potentials, and even those lower bounds are well above the experimen-
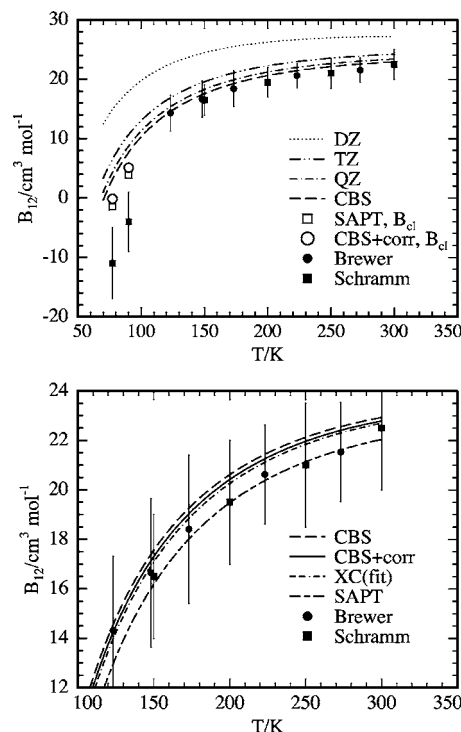

FIG. 5. Computed and measured interaction second virial coefficients. "Brewer" indicates data from Ref. 57; "Schramm" indicates data from Ref. 82. The upper panel shows results from the four CCSD(T) potentials described here, and the classical results from the CBS+corr and SAPT potentials at the two lowest experimental temperatures. The lower panel shows results from the CBS and CBS+corr potentials compared to XC(fit) and SAPT on an expanded scale.

tal ranges. Incomplete convergence of the Wigner–Kirkwood expansion therefore cannot explain all the discrepancy.

D. State-to-state integral cross sections for rotationally inelastic scattering

Antonova *et al.* measured relative state-to-state integral cross sections for rotationally inelastic He-CO scattering in a crossed-beam experiment.[3] Because the collision energies (583 and 720 cm^{-1}) in their experiment were more than 20 times the well depth, the data are sensitive almost entirely to the shape of the repulsive wall. They carried out scattering calculations and compared the data to the results from the SAPT and XC(fit) surfaces. From the amplitudes of interference oscillations in the cross sections as functions of Δj they concluded that the XC(fit) potential was too anisotropic, while the SAPT potential gave a more accurate model of the repulsive wall.

We have computed integral cross sections from the present family of surfaces for comparison with the data of Antonova *et al.* The calculations used the accurate close-coupling (CC) approach and the 2D vibrationally averaged surfaces described in Sec. II C. The MOLSCAT program of Hutson and Green,[63] with the propagator of Alexander and Manolopoulos,[64] was used. The rotational basis set included all levels with $j \leqslant 23$, and the potential was expanded in a set of 15 Legendre functions with MOLSCAT's built-in quadrature routines. At the highest energy (890 cm^{-1}), the partial wave
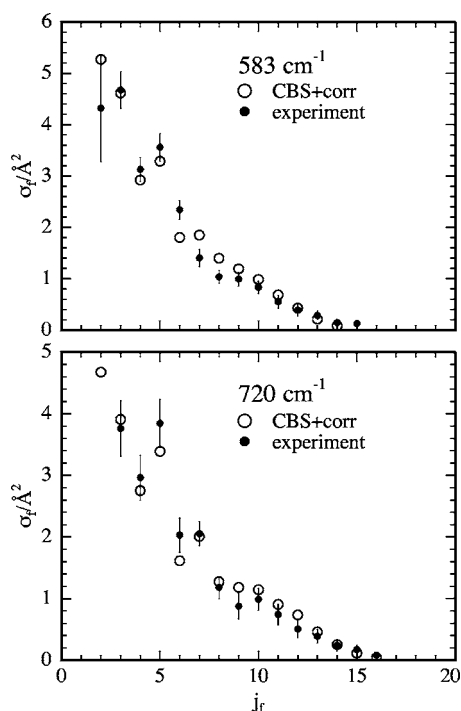
FIG. 6. Integral cross sections for rotational excitation, averaged over the initial rotational distribution of Antonova *et al.* (Ref. 3) and weighted to correct for the density-to-flux transformation. The experimental results have been scaled to match the total cross section for $j_f \geq 3$.

sum included terms up to total angular momentum quantum number 67.

These integral cross sections converged quickly with basis set. At 583 cm^{-1}, for $j=0 \rightarrow j_f$ transitions with $2 \leq j_f \leq 11$, the DAVDZ results were already within 10% of the CBS limit, and the DAVTZ results were within 5%. At $j_f = 1$ the errors were 11% for DAVDZ and 6% for DAVTZ. The experimental error bars amount to about 10% of the measured relative cross section, so comparisons with experiment are not able to distinguish among the different basis sets used here.

The cross sections computed from the CBS potential were averaged over the initial rotational state distribution and corrected for the density to flux transformation as described by Antonova *et al.* for comparison with the data. The results are shown in Fig. 6; this figure may be compared directly with Fig. 3 of Ref. 3. The CBS potential does a good job of predicting the amplitudes of the interference oscillations in the cross section, and similarly does well at predict-

ing the overall falloff with higher Δj. Its performance is very similar to that of the SAPT potential, and clearly better than that of the XC(fit) potential.

E. Rotational energy transfer rate coefficients

Smith *et al.*[4] reported infrared double-resonance measurements of rotational relaxation of CO induced by He at 296 K. These data are closely related to state-to-state rate coefficients for rotationally inelastic scattering in $v=2$ CO. They are more highly averaged than the state-to-state cross sections discussed in Sec. III D, since they are thermal quantities, but they have the advantage that they do not require a scaling factor in the comparison between theory and experiment.

We have computed a matrix of state-to-state rate coefficients from the CBS+corr surface by the methods described by Smith *et al.* For these calculations we used the 2D vibrationally averaged surface appropriate to $v=2$. A dense grid of collision energies, as described by Smith *et al.*, was used below 900 cm^{-1} to resolve the threshold structure in the cross sections for all initial states of CO with $j \leq 20$. Above 900 cm^{-1} a coarser grid was adequate. Close-coupled calculations were used at collision energies up to 1442 cm^{-1}; at energies above that, the coupled-states (CS) approximation of McGuire and Kouri[65] was used. The highest collision energy in the calculations was 1937.5 cm^{-1}, where 34 rotational levels were included in the basis set. At the highest collision energies, Legendre terms up to $\lambda = 18$ were used in the angular expansion of the potential, and they were determined by 30-point Gaussian quadrature; total angular momentum quantum numbers up to 77 were necessary to converge the partial wave expansion.

The resulting cross sections were averaged over the collision energy distribution at 296 K by the trapezoidal rule to obtain rate coefficients. Those coefficients were then used to predict the evolution of population among the $v=2$ rotational levels of CO after pumping of a particular initial level in the IR pump-probe experiment. Comparisons were made for all initial states $2 \leq j_i \leq 9$; Fig. 7 shows the results for $j_i=5$. This figure can be compared directly with Fig. 6 of Ref. 4, which shows similar curves obtained with the SAPT surface. The noisy traces in Fig. 7 are not raw data; they are experimental "population profiles," which have been obtained from the raw absorption versus time data by removing the effects of vibrational relaxation, of rotational relaxation by CO-CO
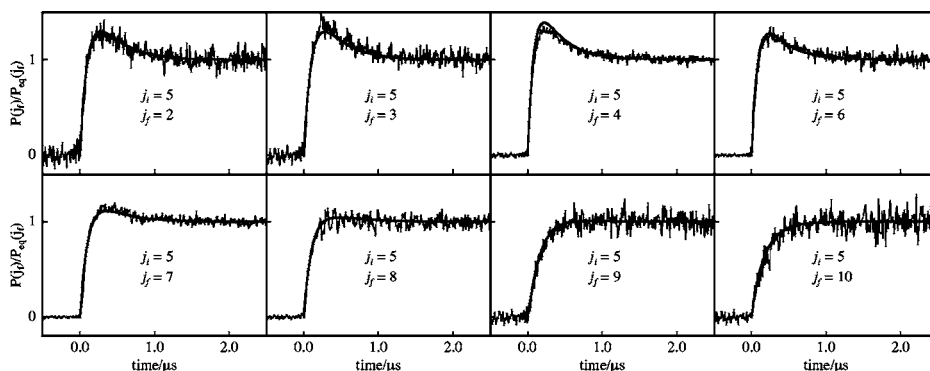

FIG. 7. Population profiles determined by IR double-resonance measurements (Ref. 4). The noisy trace in each panel is the relative population in level $v=2, j=j_f$ after pumping of $v=2, j=5$ as a function of time, where the redistribution of population is caused by collisions with ^{4}He at 296 K. The smooth trace is the population predicted by the CBS+corr surface.

collisions, and of evolution in the absorption line shape brought on by velocity relaxation. In each panel, the long-time amplitude in the experimental trace has been set to correspond to the known Boltzmann population. The information content in each trace is in the slope of the initial rise and in the shape of the approach to equilibrium.

The CBS+corr surface is able to predict the IR double-resonance data nearly quantitatively. Nowhere in the entire data set does the predicted trace differ from the experimental results by more than twice the local noise level, and usually the prediction is well within the noise. (In fact, Fig. 7 shows one of the poorer fitting initial states.) It is not surprising that the agreement is good, since the state-to-state cross sections indicated that the anisotropy on the repulsive wall was accurately described. Nonetheless, the double-resonance data do sample a much wider range of collision energies and corresponding parts of the repulsive wall.

The SAPT potential also gives excellent agreement with these data; the experiment is not able to differentiate between the two surfaces.

F. Vibrational energy transfer rate coefficients

Rate coefficients for vibrational relaxation of CO by He have been measured by Millikan[66] and by Miller and Millikan,[67] Green and Hancock,[68] Stephenson and Mosburg, Jr.,[69] and Simpson and co-workers.[70–75] These measurements probe the r_{CO} dependence of the potential; to produce a $\Delta \nu \neq 0$ transition, the colliding atom must be able to apply a force to the CO bond. The regions of large dV/dr_{CO} are all at relatively small R, but at low temperatures those regions are inaccessible, and the vibrational inelasticity arises from the weak dependence of the interaction potential on r_{CO} in the well and on the low-energy repulsive wall. Vibrational relaxation rate constants over a wide range of temperatures therefore test the r_{CO} dependence of a model potential over many of the important regions of the surface. Experimental data are available from 35 to over 2300 K.

We used the MOLSCAT program to compute state-to-state cross sections for vibrational deactivation at a wide range of energies, using the DAVTZ, DAVQZ, CBS, CBS+corr, and SAPT surfaces. The cross section calculations used the radial strength functions defined in Eq.(9), and the coupled states approximation of McGuire and Kouri.[65] (The SAPT potential is also defined in terms of a polynomial expansion in r_{CO}; we modified the original SAPT evaluation subroutine to obtain equivalent radial strength functions for comparison.) At modest collision energies the cross sections for vibrational relaxation are small, and the scattering calculations must be performed with care. Closed channels make important contributions. Table X shows the total energies we used and the corresponding basis sets. We chose these basis sets after considerable experimentation; at some energies, removal of a few closed channels can cause large errors in the cross sections.

For total energies below 3145 cm^{-1}, orbital angular momenta up to $l=40$ were included in the partial wave sum; at higher energies, the sum was extended to $l=80$. Those limits are not always adequate to converge rotationally inelastic

TABLE X. Energies and basis sets used in vibrational relaxation calculations. The basis set notation 45/29/10 means rotational levels 0–45 in $\nu=0$, 0–29 in $\nu=1$, and 0-10 in $\nu=2$ were included in the channel basis. All energies are in cm^{-1}. The energy of the $\nu=1, j=0$ level is 2143.237 cm^{-1}.

Energy range	Energy spacing	Basis set
2143-2165	0.5	45/29/10
2160-2300	10	45/29/10
2300-3145	50	45/29/10
3145-3645	50	56/48/24
3645-6145	100	56/48/24
6300-9300	500	55/55/29/9

cross sections, but they capture essentially all of the vibrationally inelastic scattering. All our comparisons to experimental data involve quantities that are averaged over rotational states so we expect no substantial contributions to the error from truncation of the partial wave sums.

To obtain rate coefficients for vibrational relaxation, we then averaged those cross sections over collision energy at each temperature according to

$$\sigma_{if}(T) = \frac{1}{(k_B T)^2} \int_0^\infty \epsilon \sigma(\epsilon) \exp\left(\frac{-\epsilon}{k_B T}\right) d\epsilon, \quad (13)$$

where ϵ is the translational energy before the collision. The integral was performed by the overlapping-parabolas method[76] up to the highest collision energy in our set of computed cross sections. Even at the highest collision energies the cross sections for vibrationally inelastic processes were still increasing rapidly with energy, though the integrand of Eq. (13) was decreasing because of the exponential factor. We therefore fit the last three points of $\sigma(\epsilon)$ to a quadratic function and used those fit coefficients to estimate analytically the high-energy tail of the integral. At temperatures below 600 K the "tail correction" was negligible, but it contributed 8% of the total rate coefficient at 939 K, 12% at 1027 K, 30% at 1310 K, and 43% at 1500 K.

To obtain the vibrational relaxation rate coefficients we then averaged over initial rotational states in $\nu=1$ according to their Boltzmann populations, and summed over all final rotational states in $\nu=0$:

$$k(T) = \left(\frac{8k_B T}{\pi \mu}\right)^{1/2} \sum_{j_i} \sum_{j_f} \frac{(2j_i+1)\exp(-E_{j_i}/k_B T)}{Q_i(T)} \sigma_{if}(T), \quad (14)$$

where E_{j_i} is the rotational energy of the $\nu=1, j=j_i$ level of CO and $Q_i(T)$ is the rotational partition function in $\nu=1$ at temperature T.

Table XI shows vibrational relaxation rate coefficients from the SAPT surface, from our four best surfaces, and from experiment. The smooth convergence with basis set is apparent in the central columns. At low temperatures, the change from the DAVTZ to the CBS+corr potential is relatively large; this is to be expected, since at low T vibrational relaxation is strongly affected by the attractive well of the potential. At higher temperatures, collisions on the repulsive wall dominate (because there it is possible to apply a much

TABLE XI. Rate coefficients for $1 \to 0$ vibrational relaxation. All entries are in units of $cm^3 \, s^{-1}$.

T/K	SAPT	DAVTZ	DAVQZ	CBS	CBS+corr	Expt.[a]	
35	1.98×10^{-20}		2.23×10^{-20}	2.90×10^{-20}	3.51×10^{-20}	3.0×10^{-20}	
40	2.25×10^{-20}		2.60×10^{-20}	3.34×10^{-20}	3.99×10^{-20}	3.7×10^{-20}	
50	3.04×10^{-20}	2.67×10^{-20}	3.63×10^{-20}	4.58×10^{-20}	5.30×10^{-20}	5.2×10^{-20}	
70	5.91×10^{-20}		7.26×10^{-20}	8.85×10^{-20}	9.73×10^{-20}	9.4×10^{-20}	
85	9.77×10^{-20}		1.20×10^{-19}	1.44×10^{-19}	1.53×10^{-19}	1.6×10^{-19}	
100	1.58×10^{-19}		1.95×10^{-19}	2.28×10^{-19}	2.38×10^{-19}	2.4×10^{-19}	
150	6.62×10^{-19}	6.54×10^{-19}	7.85×10^{-19}	8.78×10^{-19}	8.93×10^{-19}	1.0×10^{-18}	
200	2.14×10^{-18}		2.39×10^{-18}	2.62×10^{-18}	2.65×10^{-18}	3.3×10^{-18}	
250	5.69×10^{-18}		5.99×10^{-18}	6.48×10^{-18}	6.53×10^{-18}	8.9×10^{-18}	
290	1.12×10^{-17}	1.01×10^{-17}	1.13×10^{-17}	1.21×10^{-17}	1.22×10^{-17}	1.6×10^{-17}	
580	3.21×10^{-16}	2.48×10^{-16}	2.67×10^{-16}	2.80×10^{-16}	2.81×10^{-16}		4.6×10^{-16}
939	3.27×10^{-15}		2.54×10^{-15}	2.62×10^{-15}	2.63×10^{-15}	4.4×10^{-15}	3.5×10^{-15}
1027	4.95×10^{-15}	3.62×10^{-15}	3.81×10^{-15}	3.94×10^{-15}	3.94×10^{-15}	6.2×10^{-15}	5.0×10^{-15}
1310	1.46×10^{-14}		1.12×10^{-14}	1.15×10^{-14}	1.15×10^{-14}	1.8×10^{-14}	1.2×10^{-14}
1500	2.59×10^{-14}	1.90×10^{-14}	1.98×10^{-14}	2.03×10^{-14}	2.03×10^{-14}		2.0×10^{-14}

[a]The experimental results for temperatures of 290 K and below are from the compilation in Ref. 15. Above 290 K, the experimental results are from the compilation in Ref. 72; the first column of values is due to Chenery (Ref. 84), and the second is due to Millikan (Ref. 66).

stronger force to the CO bond), and the DAVTZ potential already gives a good description of the repulsive wall.

The experimental rate coefficients for vibrational relaxation span nearly six orders of magnitude. None of the rate coefficients computed from the CBS+corr surface have errors with respect to the experimentally measured results of more than 40%, and most are closer. The CBS+corr computed rate coefficients are higher than the experimental data below 85 K and lower above 150 K. By contrast, the SAPT rate coefficients are lower than the experimental values at all temperatures below 1000 K, but grow closer as the temperature increases and are within the experimental error bars above 1000 K. Rate coefficients from the CBS+corr potential therefore show slightly too little sensitivity to temperature, while those from the SAPT potential show slightly too much.

All the computed entries, including those for the SAPT surface, were obtained by the usual *l*-labeled CS approximation as described above (EWF-*j*-*l*-CSA in Krems's notation[17,18]). Our "SAPT" values differ from those presented by Krems because he used a different CS approximation that included all the diagonal terms in the body-fixed centrifugal Hamiltonian; this approximation has also been used by Banks *et al.*[77] and by Kuppermann *et al.*[78] In the discussion following the original development of the CS approximation, this version was rejected on theoretical grounds,[79,80] but Krems found that it gave good agreement with the close-coupled results of Balakrishnan *et al.* for He-CO vibrational relaxation at low temperatures.[81] We have been able to reproduce Krems's results both with his ABC3D program and with MOLSCAT, but we have chosen the more widely used *l*-labeled CS approximation in this work.

Our SAPT results also differ from those presented by Reid *et al.*[15] They used the same CS approximation we did, but they used harmonic oscillator wave functions for the vibrational motion of CO and used the same vibrational wave function for all CO rotational levels, while we have used accurate CO wave functions determined separately for each rotational level.

In Krems's studies with an alternative CS approximation,[17,18] he found that vibrational relaxation cross sections computed with the "full diagonal centrifugal term" CS approximation were larger than those computed with the *l*-labeled approximation used here and had a less steep collision energy dependence. The resulting rate coefficients therefore had a less steep temperature dependence than the SAPT rate coefficients shown above and gave better agreement with the experimental results. In limited tests at collision energies of 1000 cm^{-1} and below, we do not find evidence that the alternative CS approximation produces a similar improvement in the agreement with experiment for the CBS+corr potential.

IV. CONCLUSIONS

A hierarchical series of three-dimensional (and effective two-dimensional) potential energy surfaces has been developed for the He-CO van der Waals system. Four of these surfaces were obtained at the CCSD(T) level of theory with basis sets ranging from d-aug-cc-pVDZ to the CBS limit. The fifth corresponds approximately to a CCSDT/CBS interaction surface. The position of the global minimum and its associated well depth vary smoothly with surface quality, with the latter varying from -14.83 to -22.34 cm^{-1}. A number of properties have been calculated on most of these surfaces that included the infrared spectrum of both ^{4}He-CO and ^{3}He-CO, the interaction second virial coefficient, integral cross sections and thermal rate coefficients for rotational relaxation of CO by collisions with He, and rate coefficients for CO vibrational relaxation by He. These calculations have demonstrated that the CBS+corr potential surface has the highest accuracy of any *ab initio* surface to date and provides the best overall description of the He+CO system. In particular, use of a systematic series of surfaces clearly shows the sensitivity of different properties to the quality of the underlying interaction potential. As expected, the infrared spectrum is strongly dependent on an accurate well depth, while the second virial coefficient shows only a weak depen-

dence on the underlying interaction potential. The calculated scattering properties also smoothly vary with surface quality, e.g., the rate coefficients for vibrational relaxation (CO $v = 1 \rightarrow 0$) are already well converged with respect to surface quality at the DAVTZ level for temperatures above 250 K, but the lower-temperature rate coefficients exhibit a stronger dependence. All of the 2D and 3D potential surfaces developed in this work are available as FORTRAN 77 routines and have been deposited with EPAPS.[85]

ACKNOWLEDGMENTS

[1] S. Green and P. Thaddeus, Astrophys. J. **205**, 766 (1976).
[2] M. Thachuk, C. E. Chuaqui, and R. J. Le Roy, J. Chem. Phys. **105**, 4005 (1996).
[3] S. Antonova, A. Lin, A. P. Tsakotellis, and G. C. McBane, J. Chem. Phys. **110**, 2384 (1999).
[4] T. C. Smith, D. A. Hostutler, G. D. Hager, M. C. Heaven, and G. C. McBane, J. Chem. Phys. **120**, 2285 (2004).
[5] L. D. Thomas, W. P. Kraemer, and G. H. F. Diercksen, Chem. Phys. **51**, 131 (1980).
[6] R. Schinke and G. H. F. Diercksen, J. Chem. Phys. **83**, 4516 (1985).
[7] C. E. Chuaqui, R. J. Le Roy, and A. R. W. McKellar, J. Chem. Phys. **101**, 39 (1994).
[8] R. J. Le Roy, C. Bissonnette, T. H. Wu, A. K. Dham, and W. J. Meath, Faraday Discuss. **97**, 81 (1994).
[9] A. Dham and W. Meath, Mol. Phys. **88**, 339 (1996).
[10] A. F. Zolotoukhina and S. Kotake, J. Chem. Phys. **99**, 2855 (1993).
[11] B. Kukawska-Tarnawska, G. Chałasinski, and K. Olszewski, J. Chem. Phys. **101**, 4964 (1994).
[12] F.-M. Tao, S. Drucker, R. C. Cohen, and W. Klemperer, J. Chem. Phys. **101**, 8680 (1994).
[13] T. G. A. Heijmen, R. Moszynski, P. E. S. Wormer, and A. van der Avoird, J. Chem. Phys. **107**, 9921 (1997).
[14] R. Moszynski, T. Korona, P. E. S. Wormer, and A. van der Avoird, J. Chem. Phys. **103**, 321 (1995).
[15] J. Reid, C. Simpson, and H. Quiney, J. Chem. Phys. **107**, 9929 (1997).
[16] R. Moszynski, T. Korona, T. G. A. Heijmen, P. E. S. Wormer, A. van der Avoird, and B. Schramm, Pol. J. Chem. **72**, 1479 (1998).
[17] R. V. Krems, J. Chem. Phys. **116**, 4517 (2002).
[18] R. V. Krems, J. Chem. Phys. **116**, 4525 (2002).
[19] F. R. W. McCourt, M. A. Ter Horst, E. L. Heck, and A. S. Dickinson, Mol. Phys. **100**, 3893 (2002).
[20] F. A. Gianturco, F. Paesani, M. F. Laranjeira, V. Vassilenko, M. A. Cunha, A. G. Shashkov, and A. F. Zolotoukhina, Mol. Phys. **94**, 605 (1998).
[21] F. A. Gianturco and F. Paesani, Mol. Phys. **99**, 689 (2001).
[22] R. Kobayashi, R. D. Amos, J. P. Reid, H. M. Quiney, and C. J. S. M. Simpson, Mol. Phys. **98**, 1995 (2000).
[23] W. B. Zeimen, G. C. Groenenboom, and A. van der Avoird, J. Chem. Phys. **119**, 131 (2003).
[24] S. L. Mielke, B. C. Garrett, and K. A. Peterson, J. Chem. Phys. **116**, 4142 (2002).
[25] K. A. Peterson, S. Skokov, and J. M. Bowman, J. Chem. Phys. **111**, 7446 (1999).
[26] B. Ramachandran and K. A. Peterson, J. Chem. Phys. **119**, 9590 (2003).
[27] K. A. Peterson, J. Chem. Phys. **113**, 4598 (2000).
[28] D. E. Woon, J. Chem. Phys. **100**, 2838 (1994).
[29] D. E. Woon, T. H. Dunning, Jr., and K. A. Peterson, J. Chem. Phys. **104**, 5883 (1996).
[30] D. E. Woon, K. A. Peterson, and T. H. Dunning, Jr., J. Chem. Phys. **109**, 2233 (1998).
[31] K. A. Peterson and T. H. Dunning, Jr., Theor. Chim. Acta **400**, 93 (1997).
[32] S. F. Boys and F. Bernardi, Mol. Phys. **19**, 553 (1970).
[33] D. E. Woon and T. H. Dunning, Jr., J. Chem. Phys. **100**, 2975 (1994).
[34] T. H. Dunning, Jr., J. Chem. Phys. **90**, 1007 (1989).
[35] R. A. Kendall, T. H. Dunning, Jr., and R. J. Harrison, J. Chem. Phys. **96**, 6796 (1992).
[36] T.-S. Ho and H. Rabitz, J. Chem. Phys. **104**, 2584 (1996).
[37] K. A. Peterson, D. E. Woon, and T. H. Dunning, Jr., J. Chem. Phys. **100**, 7410 (1994).
[38] J. Noga and R. J. Bartlett, J. Chem. Phys. **86**, 7041 (1987).
[39] H.-J. Werner, P. J. Knowles, J. Almlöf *et al.*, MOLPRO, Universität Stuttgart and Cardiff University (2002).
[40] J. F. Stanton, J. Gauss, J. D. Watts *et al.*, ACES II, Quantum Theory Project, University of Florida, Gainsville, FL. Integral packages included are VMOL (J. Almlöf and P. R. Taylor), VPROPS (P. Taylor), and ABACUS (T. Helgaker, H. J. Aa. Jensen, P. Jørgensen, J. Olsen, and P. R. Taylor).
[41] T.-S. Ho and H. Rabitz, J. Chem. Phys. **113**, 3960 (2000).
[42] P. Soldan and J. M. Hutson, J. Chem. Phys. **112**, 4415 (2000).
[43] T. Hollebeek, T.-S. Ho, and H. Rabïtz, J. Chem. Phys. **106**, 7223 (1997).
[44] S. M. Kirschner and J. K. G. Watson, J. Mol. Spectrosc. **47**, 234 (1973).
[45] P. Huxley and J. N. Murrell, J. Chem. Soc., Faraday Trans. 2 **79**, 323 (1983).
[46] D. T. Colbert and W. H. Miller, J. Chem. Phys. **96**, 1982 (1992).
[47] R. J. Le Roy, University of Waterloo Chemical Physics Research Report No. CP-642R, 2001. Source code and manual available from the "Computer Programs" link on the www site http://leroy.uwaterloo.ca
[48] A. G. Maki, J. S. Wells, and D. A. Jennings, J. Mol. Spectrosc. **144**, 224 (1990).
[49] R. J. Le Roy, University of Waterloo Chemical Physics Research Report No. CP-657, 2003. Source code and manual available from the "Computer Programs" link at http://leroy.uwaterloo.ca
[50] T. Helgaker, W. Klopper, H. Koch, and J. Noga, J. Chem. Phys. **106**, 9639 (1997).
[51] J. M. Hutson, BOUND computer code, Version 5, distributed by Collaborative Computational Project No. 6 of the Science and Engineering Research Council (UK, 1993).
[52] A. Le Floch, Mol. Phys. **72**, 133 (1991).
[53] L. A. Surin, D. A. Roth, I. Pak, B. S. Dumesh, F. Lewen, and G. Winnewisser, J. Chem. Phys. **112**, 4064 (2000).
[54] M.-C. Chan and A. R. W. McKellar, J. Chem. Phys. **105**, 7910 (1996).
[55] A. R. W. McKellar, Y. Xu, W. Jäger, and C. Bissonnette, J. Chem. Phys. **110**, 10766 (1999).
[56] S. Skokov, J. Qi, J. M. Bowman, C.-Y. Yang, S. K. Gray, K. A. Peterson, and V. A. Mandelshtam, J. Chem. Phys. **109**, 10273 (1998).
[57] J. Brewer, AFOSR Technical Report MRL-2915-C, 1967. Cited in Ref. 16.
[58] B. Schramm, E. Elias, L. Kern, G. Natour, A. Schmitt, and C. Weber, Ber. Bunsenges. Phys. Chem. **95**, 615 (1991).
[59] R. T Pack, J. Chem. Phys. **78**, 7217 (1983).
[60] J. O. Hirschfelder, C. F. Curtiss, and R. B. Bird, *Molecular Theory of Gases and Liquids* (Wiley, New York, 1954).
[61] L. W. Bruch, J. Chem. Phys. **54**, 4281 (1971).
[62] L. W. Bruch, J. Chem. Phys. **55**, 5101 (1971).
[63] J. M. Hutson and S. Green, MOLSCAT computer code, Version 14, distributed by Collaborative Computational Project No. 6 of the Engineering and Physical Sciences Research Council (UK, 1994).
[64] M. H. Alexander and D. E. Manolopoulos, J. Chem. Phys. **86**, 2044 (1987).

[65] P. McGuire and D. J. Kouri, J. Chem. Phys. **60**, 2488 (1974).

[66] R. C. Millikan, J. Chem. Phys. **40**, 2594 (1964).

[67] D. J. Miller and R. C. Millikan, J. Chem. Phys. **53**, 3384 (1970).

[68] W. H. Green and J. K. Hancock, J. Chem. Phys. **59**, 4326 (1973).

[69] J. C. Stephenson and E. R. Mosburg, Jr., J. Chem. Phys. **60**, 3562 (1974).

[70] D. C. Allen, T. J. Price, and C. J. S. M. Simpson, Chem. Phys. **41**, 449 (1979).

[71] M. M. Maricq, E. A. Gregory, C. T. Wickham-Jones, D. J. Cartwright, and C. J. S. M. Simpson, Chem. Phys. **75**, 347 (1983).

[72] C. T. Wickham-Jones, H. T. Williams, and C. J. S. M. Simpson, J. Chem. Phys. **87**, 5294 (1987).

[73] G. J. Wilson, M. L. Turnidge, A. S. Solodukhin, and C. J. S. M. Simpson, Chem. Phys. Lett. **207**, 521 (1993).

[74] J. P. Reid, C. J. S. M. Simpson, and H. M. Quiney, Chem. Phys. Lett. **246**, 562 (1995).

[75] J. P. Reid, C. J. S. M. Simpson, H. M. Quiney, and J. M. Hutson, J. Chem. Phys. **103**, 2528 (1995).

[76] R. E. Jones, Sandia Laboratorie Technical Report No. SC-M-69-335, 1969. Implemented in the SLATEC program library as subroutine DAVINT.

[77] A. J. Banks, D. C. Clary, and H.-J. Werner, J. Chem. Phys. **84**, 3788 (1986).

[78] A. Kuppermann, G. C. Schatz, and J. P. Dwyer, Chem. Phys. Lett. **45**, 71 (1977).

[79] D. J. Kouri, R. Goldflam, and Y. Shimoni, J. Chem. Phys. **67**, 4534 (1977).

[80] G. A. Parker and R. T Pack, J. Chem. Phys. **66**, 2850 (1977).

[81] N. Balakrishnan, A. Dalgarno, and R. C. Forrey, J. Chem. Phys. **113**, 621 (2000).

[82] K. Vatter, H. J. Schmidt, E. Elias, and B. Schramm, Ber. Bunsenges. Phys. Chem. **100**, 73 (1996).

[83] F. A. Gianturco, N. Sanna, and S. Serna-Molinera, Mol. Phys. **81**, 421 (1994).

[84] J. A. Chenery, Ph.D. thesis, Oxford University, 1984. Cited in Ref. 75.

[85] See EPAPS Document No. E-JCPSA6-123-011529 for FORTRAN 77 routines. This document can be reached via a direct link in the online article's HTML reference section or via the EPAPS homepage (http://www.aip.org/pubservs/epaps.html).